Journal of Computational Design and Engineering xxx (xxxx) xxx

Contents lists available at ScienceDirect

Journal of Computational Design and Engineering

journal homepage: www.elsevier.com/locate/jcde

Semi-analytical flash temperature model for thermoplastic polymer spur gears with consideration of linear thermo-mechanical material characteristics

Borut Černe *, Jože Duhovnik, Jože Tavčar

Faculty of Mechanical Engineering, University of Ljubljana, Aškerčeva 6, 1000 Ljubljana, Slovenia

ARTICLE INFO

Article history:
Received 24 November 2018
Received in revised form 4 March 2019
Accepted 11 March 2019
Available online xxxx

Keywords:
Polymers
Gears
Thermal effects
Sliding friction
Contact mechanics

ABSTRACT

The temperature increase that occurs during running of a polymer gear pair can be divided into two components: the nominal and flash temperatures. The latter denotes the short-term temperature increase that takes place during a gear meshing cycle. A thorough analysis of the flash temperature yields an insight into the heat dissipation process, which also determines the nominal temperature increase. We focus here on the flash component using numerical and analytical computation tools, with which we can obtain realistic predictions of the temperature increase during a gear meshing cycle. The analysis is performed using a decoupled procedure that involves a mechanical finite element analysis, followed by a semi-analytical temperature evaluation method based on the computed mechanical response of the system. With it, we obtain an improved flash temperature model that offers an accurate representation of the real life thermo-mechanical processes taking place at the gear teeth contact interfaces.

1. Introduction

The temperature state of thermoplastic polymers plays a major role in their response to cyclic mechanical loads and the overall service life of thermoplastic components. An increased temperature at the gear contact interface can result in accelerated wear and even melting in the case of an excessive load. The temperature increase in polymers due to mechanical loads can occur as a result of self-heating due to non-elastic hysteresis losses in the material structure (Shojaei, Volgers, & Morris, 2017). However, in the case of gear systems, we consider the temperature increase to be prevalently a consequence of heat generated due to frictional processes. It is typically considered that the heat generated at the contact interface is entirely dissipated at the contact interface or in the first few microns below it (Kennedy, 1984). The frictional heat generated at the contact interface depends on three main parameters: the sliding speed, contact pressure, and coefficient of friction (COF). It is distributed among the contacting bodies in accordance with their specific material properties. The overall peak temperature rise above the ambient temperature that results from these heat losses can be described as the sum of two components: the bulk or nominal temperature and the flash temperature (Tian & Kennedy, 1993). Based on the works (Kennedy, Lu, & Baker, 2015; Tian & Kennedy, 1993), where a pin-on-disk tribological system is analysed, the bulk temperature rise stems from the repeated circular movement of the pin across the disk, which causes gradual accumulation of heat in the material. The flash temperature, as defined by Blok (1963), is the local temperature increase due to a heat source (frictional or any other) passing a body at a given speed. The works (Kennedy et al., 2015; Tian & Kennedy, 1993, 1994) follow this definition. The authors in Carslaw and Jaeger (1959) studied the temperature rise process due to moving heat sources (which, in essence, defines the flash temperature effect) extensively and laid the groundwork for the thermal analysis of many tribological systems. Some fundamental concepts developed in that work were also implemented in the model presented in the following pages. An insightful and concise description of some of these concepts is also presented in Kennedy (2001). Blok's theory was also applied to the case of gear flash temperature analysis. Some results obtained specifically for polymer gears are presented in Erhard (2006). These presented results were compared directly with the results obtained using the Hachmann–Strickle model (Hachmann & Strickle, 1966)—on which the temperature evaluation in the widely used VDI 2736 (VDI, 2014) guideline is based—and the Takanashi and Shoi (1980) model—which could essentially be defined as a nominal temperature model. These analytical evaluation methods are generally based on rather rough presumptions and, hence, can result in unrealistic results in some cases, as shown

* Corresponding author.
E-mail address: borut.cerne@lecad.fs.uni-lj.si (B. Černe).
URL: http://www.lecad.si (B. Černe).

https://doi.org/10.1016/j.jcde.2019.03.001
2288-4300/

for the model in the VDI 2736 guideline that was investigated in Beermann (2015). The evaluation of the nominal temperature as defined in the VDI guideline shows slightly more consistent results although deviations from the experimental results are still noticeable. The authors in Pogačnik and Tavčar (2015) address this subject and argue that the defined COF yield results that are somewhat inconsistent with their experimental tests, and in Pogačnik and Tavčar (2016), the authors argue that a further tuning of the model parameters is required to obtain conforming results. In Mao (2007), the author presents a numerical approach for the evaluation of the flash temperature based on the heat equation using the finite difference method. A time-dependent solution is presented wherein the flash temperature is evaluated throughout the meshing cycle of a polymer involute spur gear pair. This solution is compared to the analytical Blok's solution, which is also found to be a good approximation of the mean flash temperature. In Fernandes, Rocha, Martins, and Magalhaes (2018), a numerical model is presented for the evaluation of the flash and nominal temperature rise in polymer gears. A suitable power loss model is implemented to describe the contact-interface frictional heat pattern, which is imposed as a thermal load in a transient finite element analysis (FEA). The results of the analysis are compared with those of the existing analytical models for the nominal (Hooke, Mao, Walton, Breeds, & Kukureka, 1993) and flash temperature (Mao, 2007) rise, and for the load cases considered, the obtained results show a relatively good agreement. The aforementioned models, however, all have several limitations—they are restricted to involute gear geometries, and it is assumed that the polymer gear pair follows the theoretical meshing kinematics.

The work presented here offers an improved analysis approach, wherein we consider the effects of the mechanical properties of thermoplastic polymers and the detailed gear flank geometries on the gear meshing kinematics. These factors, along with the selected loading conditions dictate the contact pressures, sliding speeds, and consequently the generated frictional heat, which causes the flash temperature effect. The developed procedure also serves as groundwork for further analyses of the nominal temperature, which denotes the long-term temperature increase in the gear pair due to repetitive cyclic loading at each tooth pair. The same underlying principles dictate both flash and nominal temperature components, the main difference between both being the time frame of observation and the influencing factors (the nominal temperature rise is also dependent on effects such as convection and heat transfer to the inner gear structure and adjoining components). We summarise in Fig. 1 the content presented in this paper.

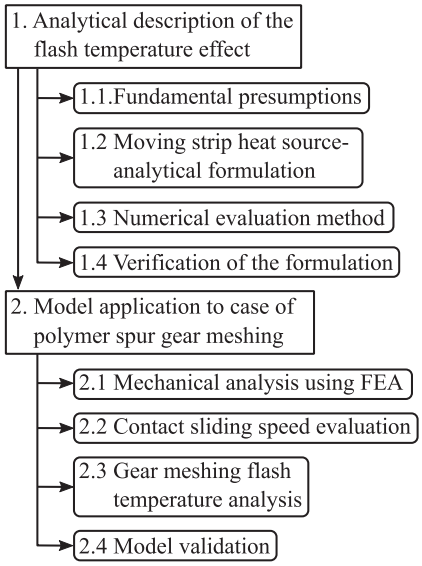

Fig. 1. Summary of the workflow structure on which the developed semi-analytical model is based.

2. General analytical formulation of the flash temperature rise due to an active heat source

2.1. Considered fundamental presumptions

The flash temperature rise that occurs during gear meshing is a rather intricate process to describe mathematically owing to the unsteady conditions prevalent during the meshing of a tooth pair. In it, we observe a constantly changing surface pressure, contact area, sliding speed, and other related parameters owing to the specific kinematics of a rotating gear pair. In order to obtain a manageable analysis procedure while still retaining a realistic flash temperature prediction, we consider the following presumptions:

i. The material properties of the polymers are independent of temperature.
ii. The heat generation is entirely due to frictional effects at the contact interface.
iii. The coefficient of friction (COF) is independent of the gear-pair running conditions, i.e., it is a constant.
iv. All frictional heat is released at the contact surfaces.
v. Convection effects do not influence the flash temperature rise.
vi. The flash temperature rise is a transient effect due to unsteady loading conditions at the contact interface.
vii. The generated frictional heat flux is distributed between the two gear teeth in contact by a specific ratio (the heat partition factor).
viii. The generated frictional heat is dissipated across the theoretical contact area.
ix. Moderate loading conditions are considered, where the system can reach a quasi-steady nominal thermal state after a given number of running cycles (see Section 4.1 for an additional clarification).

Owing to the transient conditions present during meshing, it is not feasible to obtain a fully analytical solution to describe the problem at hand appropriately. We hence turn to a combination of analytical and numerical tools, which enables us to perform a thorough analysis of the flash temperature rise that occurs at the contact interface.

2.2. Flash temperature for a moving infinite strip heat source in a semi-infinite body

A general analytical description of the flash temperature rise due to a moving heat source is presented in Appendix A. The last Eq. (A.12) presented there describes the time dependent temperature rise due to a point source moving through a body of infinite volume. Given that we are interested in modelling a frictional contact heating process, it is necessary for us to reduce the solid domain to at least a semi-infinite solid with $z \leqslant 0$. If the heat source is located at the surface of the solid, the temperature in Eq. (A.12) is simply multiplied by 2. A solution for the case wherein the heat source acting on a semi-infinite solid is expanded to an infinite line on $-\infty < y < \infty$ can be derived as follows:

$$\Delta T(\mathbf{x},t) = \frac{Q'}{4\rho c_p(\pi\alpha)^{3/2}} \int_0^t \frac{1}{(t-t')^{3/2}} \int_{-\infty}^{\infty} \times \exp\left[-\frac{(x-v(t-t'))^2 + (y-y')^2 + z^2}{4\alpha t}\right] dt', \quad (1)$$

Please cite this article as: B. Černe, J. Duhovnik and J. Tavčar, Semi-analytical flash temperature model for thermoplastic polymer spur gears with consideration of linear thermo-mechanical material characteristics, Journal of Computational Design and Engineering, https://doi.org/10.1016/j.jcde.2019.03.001

where Q' is the heat rate distribution along the line. The term

$$\int_{-\infty}^{\infty} \exp\left[-\frac{(y-y')^2}{4\alpha t}\right] dt'$$

can be solved independently by considering $y - y' := -r, 4\alpha(t-t') := a$ and using the gamma function

$$\Gamma(s) = \int_0^{\infty} (x)^{s-1} \exp(-x) dx \quad \text{or}$$

$$\Gamma(s) = \int_0^{\infty} \left(\frac{r^2}{a}\right)^{s-1} \frac{2r}{a} \exp\left(-\frac{r^2}{a}\right) dr.$$

As $\Gamma(1/2) = \sqrt{\pi}$, we obtain

$$\sqrt{\pi} = \int_0^{\infty} \frac{2}{\sqrt{a}} \exp\left(-\frac{r^2}{a}\right) dr \tag{2}$$

and hence

$$\int_{-\infty}^{\infty} \exp\left(-\frac{r^2}{a}\right) dr = \sqrt{\pi a} \tag{3}$$

Eq. (1) can then be restated as

$$\Delta T(x,z,t) = \frac{Q'}{2\pi\rho c_p \alpha} \int_0^t \frac{1}{t-t'} \exp\left\{-\frac{[x - v(t-t')]^2 + z^2}{4\alpha t}\right\} dt'. \tag{4}$$

If the heat source is a strip defined by the coordinates $x \in \{-c, c\}, y \in \{-\infty, \infty\}$, and $z = 0$, the temperature function takes the form

$$\Delta T(x,z,t) = \frac{1}{2\pi\rho c_p \alpha} \int_0^t \int_{-c}^{c} \frac{q}{t-t'} \exp\left\{\frac{[(x-x') - v(t-t')]^2 + z^2}{4\alpha t}\right\} dx' dt', \tag{5}$$

where q is the heat flux, in this case considered as being uniform and constant.

2.3. Numerical evaluation

The double integral in Eq. (5) can be solved numerically at each given (fixed) space/time point $\{x, z, t\}$ using a suitable integration algorithm. In this case, the Gauss quadrature method with $n_g = 2$ Gauss points per integration (sub) domain was implemented (Burden & Faires, 2011), with the time domain $[0, t]$ being divided into M steps and the strip width x-domain $[-c, c]$ divided into N steps. The double integral to be solved can be briefly noted as

$$\Delta T = A \int_0^t \int_{-c}^{c} f(x', t') dx' dt', \tag{6}$$

with

$$f(x', t') = \frac{q}{t-t'} \exp\left\{\frac{[(x-x') - v(t-t')]^2 + z^2}{4\alpha t}\right\} \tag{7}$$

and the constant $A = 1/(2\pi\rho c_p \alpha)$, or equivalently $A = 1/(2\pi k)$, where k is the thermal conductivity. The integration domain is then divided into M, N steps

$$\Delta T = A \sum_{j=1}^{M} \int_{t_{j-i}}^{t_j} \sum_{i=1}^{N} \int_{x_{i-1}}^{x_i} f(x', t') dx' dt'$$

The Gauss quadrature solution then takes the form

$$\Delta T \approx A \sum_{j=1}^{M} \frac{t_j - t_{j-1}}{2} \sum_{i=1}^{N} \frac{x_i - x_{i-1}}{2} \left\{\sum_{k=1}^{2} \sum_{l=1}^{2} f\left(x_i^l, t_j^k\right)\right\}, \tag{8}$$

where

$$t_j^k = \frac{(t_j - t_{j-1}) g_k + t_j + t_{j-1}}{2} \quad \text{and} \quad x_i^l = \frac{(x_i - x_{i-1}) g_l + x_i + x_{i-1}}{2}.$$

The vector $\mathbf{g} = \left(-\sqrt{3}/3, \sqrt{3}/3\right)$ (index notation g_k or g_l) denotes the gauss root coefficients. The solution presented in Eq. (5) and in numerical form in Eq. (8) can be used to model the temperature rise in a given body due to a uniform frictional heat source passing along its surface.

2.4. Verification of the solution with finite element analysis (sliding block case)

The formulation presented in Eq. (8) can be verified by comparing the obtained results with a coupled-field numerical FEA. This was performed on a simplified contact case in ANSYS Workbench as a plane stress analysis wherein a block of width 30 mm and an arbitrary thickness slides on a flat plate and releases a uniform heat flux at the contact interface (in this case we choose $q = 10^4$ W/m^2). For the plate we consider thermal and mechanical material data for the polymer polyoxymethylene POM (see Table 2), while the block only serves as a vessel for the heat release. At any given point during the sliding, a characteristic temperature pattern arises at the contact interface that is similar to that shown in Fig. 2a. A comparison of the results of the peak flash temperature for three sliding speeds is shown in Fig. 2b.

Interestingly, we can observe that a very similar pattern emerges for all three speeds where only the steady state temperature magnitude changes in value. In general, we observe fairly similar values for the developed semi-analytical method and FEA, although in some instances, the latter shows a slightly slower temperature rise. We also observe that both methods require a suitable number of time-steps (M) and a fine spatial discretisation (N) to obtain result stability. In this case the use of $M = 160$ and $N = 80$ inside the semi-analytical formulation was sufficient to obtain stable results with local errors in the range of $e_n = 0.005$ (these values can vary in correlation with the used material data and analysis parameters). In Zeller, Surendran, and Zaeh (2018) the authors also note the importance of the implementation of fine meshes for contact analysis cases, especially if high temperature gradients at the contact are present. They recommend the use of the Extended Finite Element method (XFEM) as a possible means to reduce the influence of the mesh size on the result's accuracy.

3. Application of the model to the polymer spur gear meshing case

3.1. Mechanical analysis of the gear meshing cycle using finite element analysis

In order to evaluate the flash temperature increase during a meshing cycle of an involute polymer spur gear pair, we are first required to estimate the heat flux entering the tooth flanks due to friction, which depends entirely on the conditions present at the contact interface (i.e. contact pressure, sliding speed and COF). The latter are defined by the kinematics of the system (in terms that are dependent on the gear type and geometry), selected materials, and running conditions, i.e., the torque and rotational speed. The use of polymers as construction materials typically results in a deviation from the theoretical kinematics of movement (as predicted in classical gear theory) owing to the low stiffness of the gear teeth. Consequently, the contact pressures and contact movement patterns can also vary from the theoretical predictions. In order to obtain contact response results that are as realistic as possible an FEA was performed to examine the behaviour of the

Please cite this article as: B. Černe, J. Duhovnik and J. Tavčar, Semi-analytical flash temperature model for thermoplastic polymer spur gears with consideration of linear thermo-mechanical material characteristics, Journal of Computational Design and Engineering, https://doi.org/10.1016/j.jcde.2019.03.001

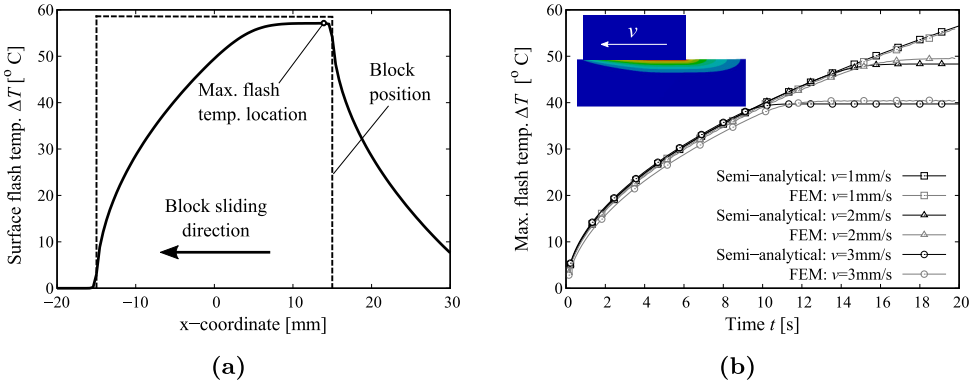

Fig. 2. Flash temperature profile at the contact interface ($z = 0$) evaluated using the semi-analytical model at $t = 20$ s for sliding speed $v = 1$ mm/s (a) and verification of the flash temperature formulation with FEA for the case of a block sliding on a flat base with constant pressure at three speeds (b).

system for a single meshing cycle. The geometry of the gears and loading conditions were selected in accordance with the experimental tests performed in Zorko, Kulovec, Tavčar, and Duhovnik (2017), where milled thermoplastic gears were tested (further description of the used testing rig presented in Duhovnik, Zorko, & Sedej (2016)). The details of the geometry of the gears are presented in Table 1.

The analysis can be reduced to a 2D plane-stress case, where the finite element (FE) mesh forms a quarter section of each gear, as shown in Fig. 3. As the objective is to simulate a full meshing cycle, we use a transient analysis, wherein the correct modelling of the contact interfaces, i.e., the teeth contact flanks, is an important aspect. In this case, an augmented Lagrange contact formulation was used with a penetration tolerance of 0.005–0.01 mm, normal stiffness coefficient value of 0.1, and radius of contact identification (named "pinball region" inside ANSYS Workbench (ANSYS, 2018)) of 0.01 mm. The radius of contact identification was crucial in achieving consistent contact response results (in general, we require a radius value that is as low as possible). A torque of 1 Nm was applied to the follower gear opposing a rotational movement by the driver gear with a frequency of $n = 1392\ \text{min}^{-1}$. The contact behaviour is observed at the middle tooth pair.

Table 1
Gear geometry parameters.

Parameter	Symbol [unit]	Value
Transmission	i [/]	1
Module	m [mm]	1
Number of teeth	z [/]	20
Pressure angle	α [°]	20
Gear width	b [mm]	6
Tip rounding	r_t [mm]	0.05
Progressive tip relief width	C_a [mm]	0.08
Diameter of tip modification	d_{Ca} [mm]	21.2294
Gear hub diameter	d_h [mm]	6

The mechanical properties of the considered materials POM and PA66 (polyamide 6/6) are presented in Table 2. A linear elastic model is considered for the analysis, as we found that the non-elastic properties of the material (i.e., viscoelasticity) do not influence the material response noticeably in the case of a single meshing cycle with moderate loads as used in our case. It is disputable whether the considered COF is selected appropriately. The author in Pogačnik (2013), for example, uses a higher value for a PA6/POM gear pair of $\mu = 0.36$. Special attention should hence be focused on the correct identification of this coefficient. For the purpose of model development, we take into consideration the value noted in Table 2, which is derived from the VDI 2736 guideline (VDI, 2014).

The analysis yields the peak contact pressure and area patterns shown in Fig. 4. Here, the points A and E define the beginning and end of the meshing cycle, the lines B and D denote the points of transition from single to double tooth-pair meshing, while the line C denotes the meshing pitch point. As might be expected, the contact response of the driver and follower gears are equal. We point out that the profile modification (i.e., tip relief) in the flank geometry has a major influence on the running conditions. If no relief is applied, the peak pressures at the beginning and end of the meshing cycle could increase significantly. A study of this effect is presented in the discussion section. Furthermore, the values of the pressures at the pitch points were compared with the analytical results based on the Hertz contact theory (Maitra, 2001; Williams & Dweyer-Joyce, 2000), and it was found that the values coincide very well here (deviations $< 3\%$).

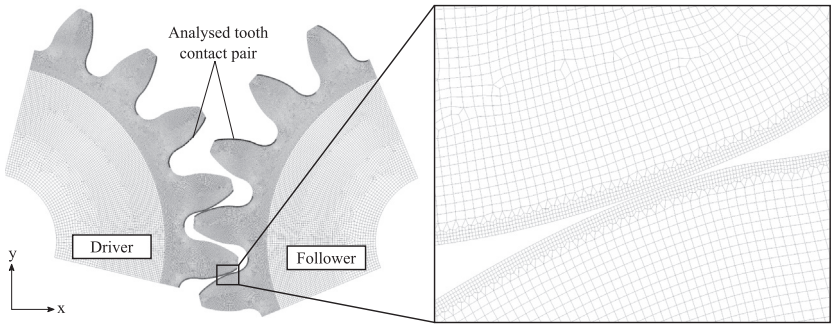

Fig. 3. Spur gear pair FE mesh.

Please cite this article as: B. Černe, J. Duhovnik and J. Tavčar, Semi-analytical flash temperature model for thermoplastic polymer spur gears with consideration of linear thermo-mechanical material characteristics, Journal of Computational Design and Engineering, https://doi.org/10.1016/j.jcde.2019.03.001

Table 2
Mechanical parameters of the considered materials based on available technical datasheets.

Parameter	Symbol [unit]	Driver gear TECAFORM AH natural (POM-C); Ensinger	Follower gear TECAMID 66 natural (PA 66); Ensinger (Matweb)
Density	ρ [kg/m^3]	1410	1140
Elastic modulus	E [MPa]	2800	2410
Tensile yield strength	R_m [MPa]	67	80
Poisson ratio	v [/]	0.35	0.4
Specific heat	c_p [J/(kg K)]	1400	1670
Thermal conductivity	k [W/(mK)]	0.39	0.37
COF (VDI, 2014)	μ [/]	0.18 (dry running)	

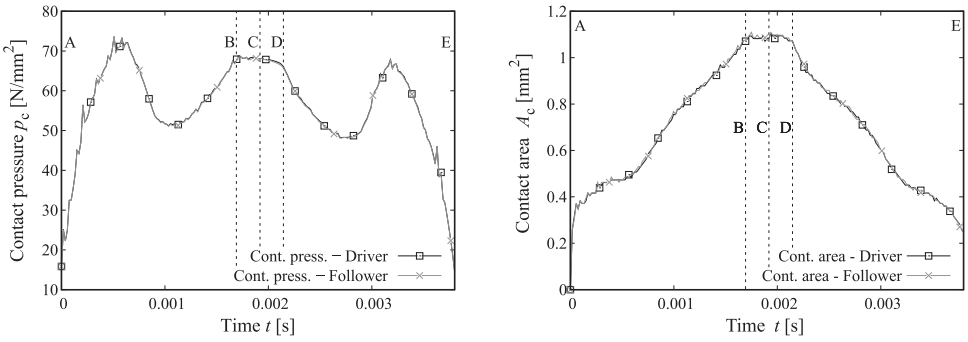

(a) Peak contact pressure. (b) Contact area.

Fig. 4. Computed peak contact pressure and contact area for a meshing cycle of a POM-PA66 polymer spur-gear pair with torque $M_t = 1$ Nm and $n = 1392$ min^{-1}.

The frictional heat flux generated at the contact interface is also a function of the sliding speed. The contact movement of a gear pair is actually a relatively complex combination of sliding and rolling. It is the sliding component, however, that is considered to be the part of the contact movement that determines the degree of frictional heat loss. In order to evaluate the sliding speed data (without the influence of the rolling part of the contact movement), a custom algorithm was developed that could extrapolate these data from the computed FE results. We can export the FEA results comprising the contact stress and deformation/displacement computed at the contact interface. The sliding speed is then evaluated by observing how the relative distance between two peak stress FE nodes (Fig. 5a) at the contact interface changes with time. At each time point, we evaluate the actual positions of the S contact interface nodes on both the driver and follower gears as

$$\mathbf{x}_r = \mathbf{x}_0 + \mathbf{u}, \quad \text{for} \quad \mathbf{x}_r = \{X_1^r, Y_1^r, X_2^r, Y_2^r, \ldots, X_S^r, Y_S^r\}.$$

$\mathbf{x}_r$ is hence the vector of the deformed/displaced nodal coordinates as a sum of the initial locations $\mathbf{x}_0$ and displacement magnitudes $\mathbf{u}$ in the x and y directions. We then find the peak stress nodes on both the contact surfaces and evaluate their relative distance vector $\mathbf{r}_d = (X_d, Y_d)$ (see Fig. 5b below).

The vector $\mathbf{r}_d$ also defines the x-axis of a local coordinate system. At the following time point, we reassess the relative distance vector of the same two nodes. Owing to the rotational movement of the gears, the local coordinate system shifts by an angle of $\Delta\varphi$. The shifted vector is denoted by $\mathbf{r}'_d = (X'_d, Y'_d)$. By co-aligning the two vectors using the coordinate system rotation $\mathbf{r}_d \rightarrow \mathbf{r}_{d,r} = (X_{d,r}, Y_{d,r})$, where

$$X_{d,r} = X_d \cdot \cos(\Delta\varphi) + Y_d \cdot \sin(\Delta\varphi) \quad \text{and} \quad Y_{d,r} = -X_d \cdot \sin(\Delta\varphi) + Y_d \cdot \cos(\Delta\varphi), \tag{9}$$

we can then define the total relative sliding movement and sliding velocity at the current time point as

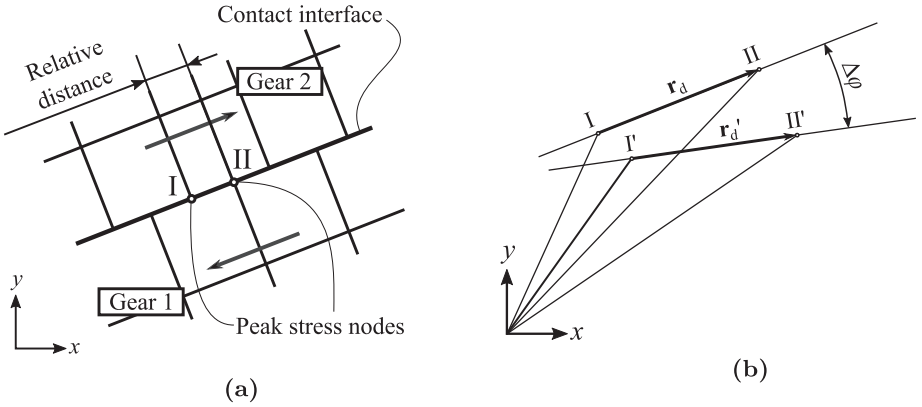

(a) (b)

Fig. 5. Relative tangential distance between peak stress nodes *I* and *II* (a) and relative distance vector shift during a given time step (b).

Please cite this article as: B. Černe, J. Duhovnik and J. Tavčar, Semi-analytical flash temperature model for thermoplastic polymer spur gears with consideration of linear thermo-mechanical material characteristics, Journal of Computational Design and Engineering, https://doi.org/10.1016/j.jcde.2019.03.001

$$\mathbf{s}_\mathrm{d} = \mathbf{r}_\mathrm{d,r} - \mathbf{r}'_\mathrm{d} \;\Rightarrow\; v_\mathrm{s} = \frac{|\mathbf{s}_\mathrm{d}|}{\Delta t}. \tag{10}$$

The sliding movement $\mathbf{s}_\mathrm{d}$ is hence defined as a change in the relative distance between the two observed nodes at two adjacent time-points. The results of the presented sliding velocity evaluation procedure are shown in Fig. 6. One interesting occurrence visible in the computed speed pattern is the speed "jump" that occurs immediately after the transition from single to double tooth-pair meshing takes place (line D). This effect was observed to be due to the load redistribution occurring during this transition, where the load drop at the observed tooth-pair results in a slight contact slip. The presented evaluation procedure typically produces a certain noise in the computed speed, which can be attributed to numerical instabilities at the contact. The signal can be smoothed out to a certain degree using a suitable signal filtering method as shown in the graph. In this case, the Savitzky–Golay (Savgol) (Savitzky & Golay, 1964; Steiner, Termonia, & Deltour, 1972) method was used. Even though this approach might, in some cases, result in a better stability in the flash temperature evaluation presented in the following sections, it was found that, for the considered gear system, no substantial benefits arose if the filtered signal was used instead of the directly computed one.

3.2. Evaluation of the flash temperature rise during gear meshing

Using the presented procedures, we obtain all the data necessary for the evaluation of the flash temperature. In the solution shown in Eq. (5), we consider steady state conditions, wherein the generated heat flux and contact area are constant. In the case of gear meshing, both these quantities become time-dependent functions. Given the rounded (almost parabolic) shape of the involute, we define the contact pressure in terms of Hertz theory (as presumed also in Fernandes et al., 2018; Li, Zhai, Tian, & Luo, 2018; Mao, 2007). Given the peak contact pressure p_c and contact half-width c, we can describe the time-dependent pressure distribution $p(x,t)$ as a semi-elliptical function (Williams & Dweyer-Joyce, 2000). In addition, on considering the sliding speed v_s evaluated as shown in Fig. 6, we can formulate the frictional heat flux as the function

$$q(x,t) = \mu \cdot v_\mathrm{s}(t) \cdot p(x,t) = \mu \cdot v_\mathrm{s}(t) \cdot p_\mathrm{c}(t) \left[1 - \frac{x^2}{c(t)^2}\right]^{\frac{1}{2}}, \tag{11}$$

where μ denotes the coefficient of friction (COF). The generated heat flux is then distributed among the two tooth flanks in contact, i.e., $q = q_\mathrm{d} + q_\mathrm{f}$ (indices d and f denote the driver and follower gear teeth, respectively). A heat partitioning ratio ψ can be used to describe the distribution such that $q_\mathrm{d} = \psi \cdot q$ and $q_\mathrm{f} = (1-\psi)\cdot q$.

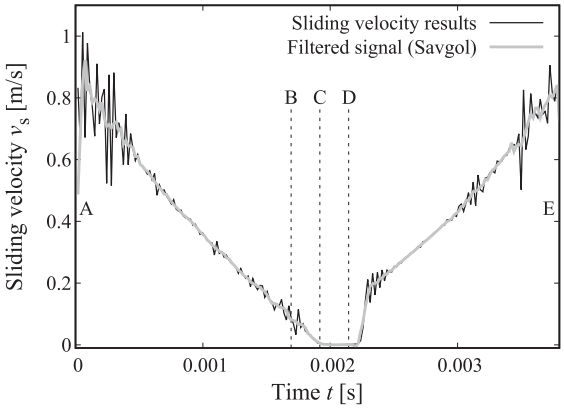

Fig. 6. Sliding velocity pattern evaluated from the gear meshing and FEA results.

Under steady state conditions, the ratio is typically a function of the location (Bansal & Streator, 2011; Bos & Moes, 1995; Kennedy et al., 2015), i.e., $\psi = \psi(x)$ for the case of a moving strip source. As noted in Kennedy, Plengsaard, and Harder (2006), for transient problems, the ratio becomes time dependent, i.e., $\psi = \psi(t)$. The authors in Sun, Sawley, Stone, and Teter (1998) show that, in a transient case, the ratio can be considered to be constant across the contact profile and, hence, only time dependent if the heat flux is also uniform across the profile. As we consider a Hertzian pressure distribution here, it is more reasonable to assume a spatial dependence of the partitioning factor, as is adopted for a 3D steady state case in Ling, Lai, and Lucca (2002). In all the cited works, the ratio is evaluated by presuming that the flash temperature at the contact interface ($z = 0$) is equal in both the sliding bodies, i.e.,

$$\Delta T_\mathrm{d}(-c(t) < x < c(t), z = 0, t) = \Delta T_\mathrm{f}(-c(t) < x < c(t), z = 0, t). \tag{12}$$

Considering Eqs. (5) and (11) and a partitioning factor $\psi(x,t)$, we obtain for the driver gear,

$$\Delta T_\mathrm{d}(x,z,t) = \frac{1}{2\pi\rho_\mathrm{d} c_\mathrm{p}^\mathrm{d} \alpha_\mathrm{d}} \int_0^t \int_{-c(t')}^{c(t')} \psi(x',t') \frac{\mu \cdot v_\mathrm{s}(t') \cdot p_\mathrm{c}(t')}{t - t'} \left[1 - \frac{(x')^2}{c(t')^2}\right]^{\frac{1}{2}} \exp\left\{-\frac{[(x-x') - v_\mathrm{s}(t')(t-t')]^2 + z^2}{4\alpha_\mathrm{d}(t-t')}\right\} dx'dt', \tag{13}$$

or, as shortened according to Eq. (6),

$$\Delta T_\mathrm{d} = A_\mathrm{d} \int_0^t \int_{-c(t')}^{c(t')} \psi(x',t')\, f_\mathrm{d}(x',t') dx'dt'. \tag{14}$$

Similarly, for the follower gear, we obtain

$$\Delta T_\mathrm{f} = A_\mathrm{f} \int_0^t \int_{-c(t')}^{c(t')} [1 - \psi(x',t')]\, f_\mathrm{f}(x',t') dx'dt'. \tag{15}$$

As shown in Fig. 4, the contact width during gear meshing is not constant, and thus, the integration bounds are also time dependent, i.e., $-c(t') < x' < c(t')$. Using Eq. (8), we can obtain the Gauss quadrature numerical formulations for both the contacting bodies

$$\Delta T_\mathrm{d}(x_p,t_r) \approx \sum_{j=1}^{M}\sum_{i=1}^{N} \tilde{\psi}_{ij} \underbrace{\sum_{k=1}^{2}\sum_{l=1}^{2} A_\mathrm{d} \frac{t_j - t_{j-1}}{2} \frac{x_i^k - x_{i-1}^k}{2} f_\mathrm{d}\left(x_p, t_r, x_i^{lk}, t_j^k\right)}_{F_{ijpr}^\mathrm{d}}, \tag{16}$$

$$\Delta T_\mathrm{f}(x_p,t_r) \approx \sum_{j=1}^{M}\sum_{i=1}^{N} \left(1 - \tilde{\psi}_{ij}\right) \underbrace{\sum_{k=1}^{2}\sum_{l=1}^{2} A_\mathrm{f} \frac{t_j - t_{j-1}}{2} \frac{x_i^k - x_{i-1}^k}{2} f_\mathrm{f}\left(x_p, t_r, x_i^{lk}, t_j^k\right)}_{F_{ijpr}^\mathrm{f}}, \tag{17}$$

where the indices p and r denote the space/time points of evaluation of the integral. The factor $\tilde{\psi}_{ij} = \tilde{\psi}(x_i, t_j)$ is evaluated at each integration subinterval $x_{i-1} < x < x_i, t_{j-1} < t < t_j$, and

$$x_i^k = x_i\left(t_j^k\right) \quad \text{and} \quad x_i^{lk} = x_i^l\left(t_j^k\right) = \frac{1}{2}\left[(x_i^k - x_{i-1}^k) g_l + x_i^k + x_{i-1}^k\right].$$

Considering Eq. (12), we find that at space–time evaluation point (x_p, t_r), the following holds.

$$\sum_{j=1}^{M}\sum_{i=1}^{N} \left[\tilde{\psi}_{ij} F_{ijpr}^\mathrm{d} - \left(1 - \tilde{\psi}_{ij}\right) F_{ijpr}^\mathrm{f}\right] = 0 \tag{18}$$

and

$$\sum_{j=1}^{M}\sum_{i=1}^{N} \left[F_{ijpr}^\mathrm{d} + F_{ijpr}^\mathrm{f}\right] \tilde{\psi}_{ij} = \sum_{j=1}^{M}\sum_{i=1}^{N} F_{ijpr}^\mathrm{f}.$$

Please cite this article as: B. Černe, J. Duhovnik and J. Tavčar, Semi-analytical flash temperature model for thermoplastic polymer spur gears with consideration of linear thermo-mechanical material characteristics, Journal of Computational Design and Engineering, https://doi.org/10.1016/j.jcde.2019.03.001

The elements F^{d}_{ijpr} and F^{f}_{ijpr} can be used to form a square matrix, wherein for each x_p, t_r (forming matrix direction 1), we evaluate the necessary integral values at points x_i, t_j. On arranging the $\tilde{\psi}_{ij}$ factors in a vector, we obtain the linear system of equations

$$[\mathbf{F}_{\mathrm{d}} + \mathbf{F}_{\mathrm{f}}]\{\tilde{\boldsymbol{\psi}}\} = [\mathbf{F}_{\mathrm{f}}]\{\mathbf{j}\}, \tag{19}$$

where on the right hand side the resulting vector is a sums of all the i,j elements at the follower gear contact interface, which in index notation translates to $F_{ijpr}j_{ij}$ ($\mathbf{j}$ or j_{ij} is formed as a vector of all ones). A system constructed in this manner has an asymmetric form and is generally ill-posed, which results in substantial solver stability issues. A solution to this is to reformulate the matrices in a symmetric form using $\mathbf{F} \rightarrow \left(\mathbf{F} + \mathbf{F}^T\right)/2$; hence

$$\left[\frac{\mathbf{F}_{\mathrm{d}} + \mathbf{F}_{\mathrm{d}}^T}{2} + \frac{\mathbf{F}_{\mathrm{f}} + \mathbf{F}_{\mathrm{f}}^T}{2}\right]\{\tilde{\boldsymbol{\psi}}\} = \left[\frac{\mathbf{F}_{\mathrm{f}} + \mathbf{F}_{\mathrm{f}}^T}{2}\right]\{\mathbf{j}\}. \tag{20}$$

The flash temperature can now be calculated using Eqs. (16) and (17), and the data can be evaluated from the FEA. The asymmetric system in Eq. (19) only yielded fairly reasonable results with a least squares (LS) residual minimisation algorithm with singular value decomposition (SVD) factorisation (LS–SVD from here on). The DGELSD routine contained in the LAPACK library (Anderson et al., 1999) was implemented to perform the computation using a rank condition number $r_{\mathrm{c}} = 10^{-3}$. Furthermore, the symmetric system in Eq. (20) can be solved using a less demanding LU factorisation (LAPACK DGESV algorithm). Fig. 7a shows the flash temperature pattern with partitioning coefficients evaluated using the described algorithms. As expected, the LS–SVD algorithm implemented with the symmetric system yields the most stable results. In Fig. 7b, we plot the results for the symmetric system evaluation using the LS–SVD solver, where we compare the evaluated results of each of the contact bodies. The results show good conformity, while the partitioning factor fluctuates stably at approximately 0.51, with the largest oscillations occurring where the sliding speed is the least stable, i.e., at the beginning, middle, and end of the cycle (see Fig. 6).

Given that the evaluation of the ψ factor as described is computationally demanding, especially for a large number of integration steps, we seek to simplify the evaluation as much as possible. From this standpoint, we attempt to define the factor as being only time dependent, i.e., $\psi = \psi(t)$. In accordance with Eq. (14), we obtain, in this case,

$$\Delta T_{\mathrm{d}} = A_{\mathrm{d}} \int_0^t \bar{\psi}(t') \int_{-c(t')}^{c(t')} f_{\mathrm{d}}(x', t') dx' dt', \tag{21}$$

where $\bar{\psi}(t')$ denotes the partitioning averaged across the contact interface. The Gauss quadrature solution for both bodies in contact now takes the form

$$\Delta T_{\mathrm{d}}(x_p, t_r) \approx \sum_{j=1}^{M} \bar{\psi}_j \underbrace{\sum_{i=1}^{N}\sum_{k=1}^{2}\sum_{l=1}^{2} A_{\mathrm{d}} \frac{t_j - t_{j-1}}{2} \frac{x_i^k - x_{i-1}^k}{2} f_{\mathrm{d}}\left(x_i^{lk}, t_j^k\right)}_{G^{\mathrm{d}}_{jpr}},$$

$$\Delta T_{\mathrm{f}}(x_p, t_r) \approx \sum_{j=1}^{M} (1 - \bar{\psi}_j) \underbrace{\sum_{i=1}^{N}\sum_{k=1}^{2}\sum_{l=1}^{2} A_{\mathrm{f}} \frac{t_j - t_{j-1}}{2} \frac{x_i^k - x_{i-1}^k}{2} f_{\mathrm{f}}\left(x_i^{lk}, t_j^k\right)}_{G^{\mathrm{f}}_{jpr}}, \tag{22}$$

where $\bar{\psi}_j = \bar{\psi}(t_j)$ is an average value evaluated across the contact interface for every time point in the computation. In order to evaluate each discrete value $\bar{\psi}_j$ at a specific time point, we are required to sum up all the integral values across the x_p dimension, i.e.,

$$G^{\mathrm{d}}_{jr} = \sum_{p=1}^{N} G^{\mathrm{d}}_{jpr} \quad \text{and} \quad G^{\mathrm{f}}_{jr} = \sum_{p=1}^{N} G^{\mathrm{f}}_{jpr}.$$

Alternatively we could also define these two tensors using the Kronecker delta tensor δ_{ip} and F^{d}_{ijpr} and F^{f}_{ijpr} as

$$G^{\mathrm{d}}_{jr} = F^{\mathrm{d}}_{ijpr}\delta_{ip} \quad \text{and} \quad G^{\mathrm{f}}_{jr} = F^{\mathrm{f}}_{ijpr}\delta_{ip}. \tag{23}$$

In this manner, we can construct a square matrix of integration elements for both the contacting bodies (denoted here as $\mathbf{G}_{\mathrm{d}}$ and $\mathbf{G}_{\mathrm{f}}$); in this case, the number of elements is equal to the number of analysis time steps (hence, we obtain an $M \times M$ matrix). The matrices can be transformed into a symmetric form as shown in Eq. (20), from which the following system of equations can be obtained.

$$\left[\frac{\mathbf{G}_{\mathrm{d}} + \mathbf{G}_{\mathrm{d}}^T}{2} + \frac{\mathbf{G}_{\mathrm{f}} + \mathbf{G}_{\mathrm{f}}^T}{2}\right]\{\bar{\boldsymbol{\psi}}\} = \left[\frac{\mathbf{G}_{\mathrm{f}} + \mathbf{G}_{\mathrm{f}}^T}{2}\right]\{\mathbf{j}\}. \tag{24}$$

Applying the partitioning factor evaluated in this manner (again using the LS–SVD solver), we can obtain the results as presented in Fig. 8a. As shown, the emerging temperature pattern is the same as that for the space-and-time-dependent partitioning $\psi(x,t)$; however, the use of this approach offers improved stability and a substantially reduced computation time. In all our polymer gear temperature evaluations we used $M = 203$ time steps and a spatial discretisation of $N = 20$ steps. In this case the evaluation time for the $\bar{\psi}(x_i, t_j)$ factor using the LS-SVD algorithm was $t_{\mathrm{e1}} = 74.95$ s,

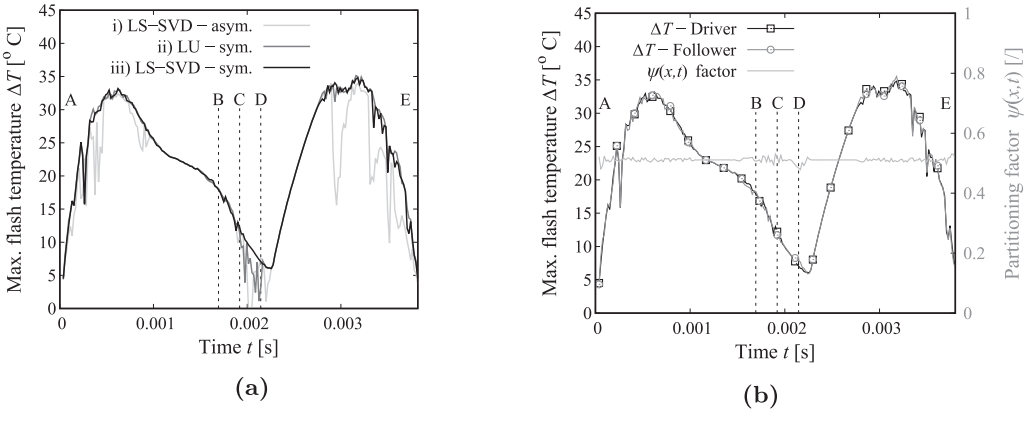

Fig. 7. Flash temperature results: comparison of the results using various solver algorithms: (i) LS–SVD solver for the asymmetric system of Eqs. (19); (ii) LU factorisation for the symmetric system (20); (iii) LS–SVD solver for the symmetric system (a); evaluation for both bodies in contact with LS–SVD algorithm for the symmetric system with evaluated partitioning coefficient ψ values (b).

Please cite this article as: B. Černe, J. Duhovnik and J. Tavčar, Semi-analytical flash temperature model for thermoplastic polymer spur gears with consideration of linear thermo-mechanical material characteristics, Journal of Computational Design and Engineering, https://doi.org/10.1016/j.jcde.2019.03.001

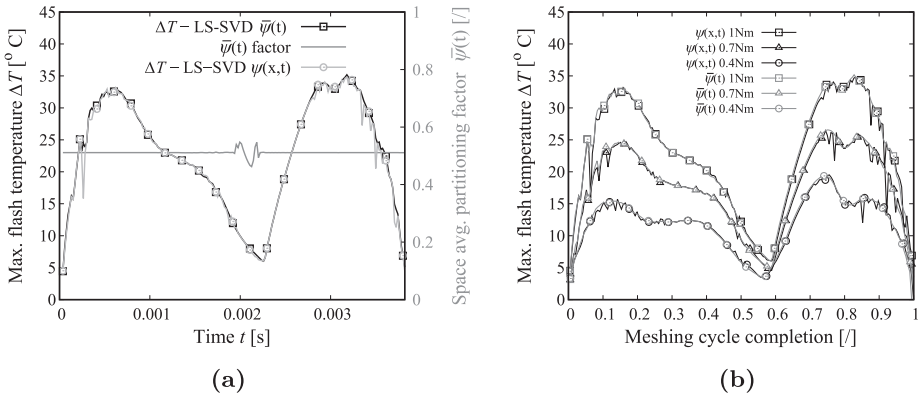

Fig. 8. Flash temperature comparison between results using partitioning factor evaluation $\psi(x,t)$ and space-averaged $\bar{\psi}(t)$ (a) and evaluation of the flash temperature for three load conditions with a comparison between the use of $\psi(x,t)$ and averaged $\bar{\psi}(t)$ partitioning factors, all evaluated using the LS–SVD solver (b).

Table 3
Load cases considered for flash temperature evaluation.

	Torque [Nm]	Running speed [min^{-1}]
Load case 1	0.4	1458
Load case 2	0.7	1428
Load case 3	1	1392

while for the space-averaged $\bar{\psi}(t_j)$ the evaluation time was merely $t_{e2} = 0.0156$ s (a reduction by roughly a factor of 4800 was hence obtained using $\bar{\psi}(t_j)$).

In addition, we can evaluate the temperature response at three gear running conditions, as noted in Table 3. We thus obtain the flash temperature plots as shown in Fig. 8b. As expected, a noticeable drop in the flash temperature is observed for decreased loads. Both the partitioning factor evaluation methods, however, show stable results, with the space-averaged $\bar{\psi}(t)$ producing relatively smoother result curves.

Both methods of evaluation of the partitioning factor, i.e., by considering a location/time dependent factor $\psi(x,t)$ and a space-averaged time dependent factor $\bar{\psi}(t)$, hence yield very similar results. The stability and computational efficiency of the implementation of the space-averaged $\bar{\psi}(t)$ makes the procedure more advantageous as compared to the use of $\psi(x,t)$, and thus, we recommend the use of the former.

4. Discussion

4.1. Critical examination of the model

In real life gear meshing conditions, the real contact area at the interface (see Myshkin, Petrokovets, & Kovalev, 2005; Persson, 2000) would be much smaller than the theoretical area considered in our computations, and thus, the actual local temperature at the micron level would definitely be higher than that evaluated by the model. The estimation of the real contact area is dependent on many factors and is hence difficult to perform. Its effect could likely be modelled by the inclusion of an additional factor in the definition of the frictional heat flux, but it should then be evaluated experimentally.

Furthermore it is possible that the COF is not constant, but a function of different parameters such as sliding velocity or temperature. While a velocity dependence would be easily implemented in our model, a temperature dependence of the COF would result in a nonlinear form of the model, for which a suitable iterative computational procedure would be required in order to perform the temperature evaluation. A thorough characterisation of the COF for the chosen material pairs will be performed in the near future in order to obtain a clearer picture on this point.

An additional point that would require special attention is the influence of the rolling friction on the overall temperature rise in the gear teeth. As noted in Wannop and Archard (1973), rolling friction due to hysteresis losses in the sub-surface region of the material can result in significant increases in the sub-surface temperatures of the rolling bodies, which can also induce wear and damage of such components. As also described in Greenwood, Minshall, and Tabor (1961), even for elastic incompressible materials such as rubber, we observe substantial energy losses due to hysteresis during rolling, which is a consequence of the specific shear stress patterns that occur below the contact interface. Based on a theory similar to the one used in this work, the authors in Wannop and Archard (1973) were able to evaluate the temperature increase below the contact surface. They noted that a distinction between the flash temperature and hysteresis temperature increase due to rolling can be made, as the former occurs predominantly in a very thin layer at and below the contact surface, while heating due to rolling hysteresis occurs comparatively deeper beneath the surface. The authors in Scaraggi and Persson (2014) also present a numerical model for the evaluation of the rolling friction in the case of a linear viscoelastic solid described by a Prony series, which can also be applied to thermoplastic polymers. In a gear meshing cycle, the rolling is generally especially pronounced around the pitch point, where we have observed that the flash temperatures are the lowest. We do not expect that the rolling friction would significantly influence the maximal temperature increase at the contact interface, but it might play a significant role in the overall long-term nominal temperature increase in the gear teeth.

As presented in Section 2.4, it is possible to use the FEA software to perform a coupled field analysis where the flash temperature can be directly evaluated. In the case of gear meshing, however, we observed that the software doesn't differentiate suitably between the sliding (which causes the frictional heat losses) and rolling, therefore leading to somewhat different heat dissipation patterns from the ones evaluated in our model. Furthermore, the future goal of this work is also to perform a thorough analysis of the long term nominal temperature rise and in this case it is not feasible to perform a direct coupled field analysis, as this would require simply too extensive computational resources (the nominal temperature increase occurs over a vast number of running cycles). Instead we intend to use the results obtained from the here presented work to define accurately the heat losses due to friction during one meshing cycle and translate these data to a suitable input function in order to perform a long term thermal analysis.

Please cite this article as: B. Černe, J. Duhovnik and J. Tavčar, Semi-analytical flash temperature model for thermoplastic polymer spur gears with consideration of linear thermo-mechanical material characteristics, Journal of Computational Design and Engineering, https://doi.org/10.1016/j.jcde.2019.03.001

An additional point that should be addressed is the range of loads for which the model is applicable. For moderate loads, the gear system reaches a state that can be considered as steady in the frame of the applied running times. In such cases, the gearing kinematics are generally preserved, and the model should yield realistic results. However, if excessively high loads are used, a substantial strain accumulation occurs owing to the viscous properties of polymers. This inevitably results in a further deviation from the ideal gearing kinematics, higher contact loads, and, consequently, increased local contact temperatures (which also negatively affect the mechanical properties of these materials). The limits below which the load conditions can still be considered as moderate depend on the materials selected, the gear geometry used, and also on the required lifetime of the system. For example, the 1Nm load used in our exemplary case is already on the upper limit of what we'd consider a moderate load, as the contact stresses exceed 70 MPa and, as observed from experiments, a (quasi) steady state in the system is reached only for a short period before substantial degradation and failure takes place (refer to Zorko et al., 2017). The conditions used by Mao in the work we used for the validation of our model are, given the evaluated temperatures and stresses, in our opinion above the limit of real life industrial applications.

An identified weak point of our model is that it does not consider the effect of temperature on the properties of polymers. A variation in temperature has an effect on the mechanical and thermal properties of thermoplastics ranging from the stiffness, thermal conductivity, specific heat, specific volume etc. Especially for thermoplastics with a glass transition temperature T_g above the environmental application temperature (like PA66) it is important to observe the effect of the temperature rise during gear running. If this limit is surpassed a substantial increase in material ductility is observed which can lead to deviations in the resulting contact pressure patterns and overall flash temperature response. We note however that the flash temperature increase itself takes place in a very narrow band below the contact surface and would hence presumably influence the overall mechanical response of the gears only slightly. This point should be considered more carefully in the nominal temperature analysis where the temperature gradients are present throughout the gear's structure.

A further possible upgrade to the model would be to simulate inside the mechanical analysis the effect of the applied manufacturing tolerances to the gear design. As shown in Section 4.3 the deviations from the theoretical tooth profile geometry (e.g. with the implementation of tip profile corrections) can influence very substantially the generated heat losses and the resulting flash temperatures. In light of these findings it would be recommendable to analyse also the effect of unwanted geometric deviations as a result of the manufacturing process. As part of our future work, we intend to tackle this aspect of the problem as well.

4.2. Overview of the developed analysis structure

We present below, in Fig. 9, a schematic representation of the developed analysis procedure. We hence favour the use of the averaged time-dependent partitioning factor $\bar{\psi}(t)$ as it proved to offer the most efficient, stable and viable solution in the identification of the flash temperature. The here presented procedure also provides the groundwork for the analysis of the long term nominal temperature evaluation. The latter is dependent on the same processes that define the flash temperature rise, so the results obtained here and the underlying theoretical background presented in the previous pages, along with a consideration of the structural and convective heat transfer effects on the gear train, will enable an analysis of the long term temperature rise.

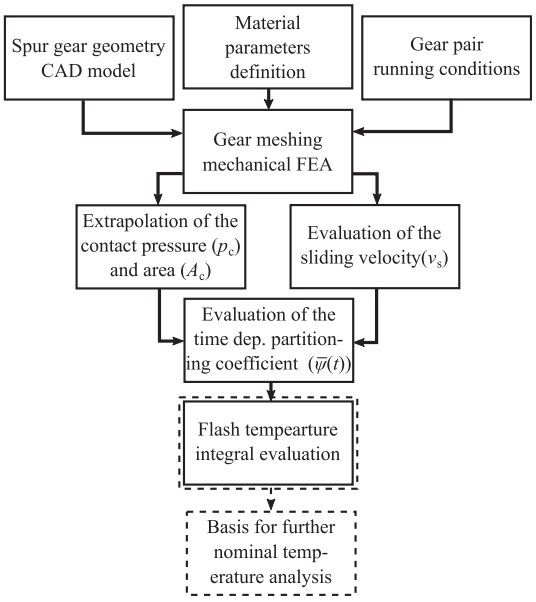

Fig. 9. Developed flash temperature analysis scheme.

4.3. Validation with results from literature

In order to validate the presented model, we turn to the results available in the literature. As previously mentioned, the work (Mao, 2007) presents a flash-temperature evaluation procedure using a finite difference computation scheme for a polymer gear pair fabricated using POM. On considering the same material properties, geometry parameters, and loading conditions as those in the cited work (refer to Table 4) in our model, some interesting observations were made. Along with the theoretical gear geometry (generated using the software KissSoft), we performed the analyses also for two types of progressive teeth profile modifications, with different tip relief sizes C_a starting at diameters d_{Ca} (using a curvature factor 10).

As shown in Fig. 10a, the tip alteration influences the contact pressures substantially. For the unmodified geometry, we can observe very high peak stresses at the beginning and end of the meshing cycle, which are due to a minor jamming of the teeth. Furthermore, the pressure at the pitch point is slightly lower for the unmodified geometry than for the altered tip geometries. This is because, in the first case, the gears do not exhibit single-tooth contact at the pitch point, and we instead always have double- or even

Table 4
Gear geometry and material parameters used for validation procedure as defined in Mao (2007) and Mao (1993) (gears with 30 teeth are used and not 20 as stated in Mao (2007))

Parameter	Symbol [unit]	Value
Module	m [mm]	2
Number of teeth	z	30
Pressure angle	α [°]	20
Gear width	b [mm]	17
Tip rounding	r_t [mm]	0.07
Profile modification	Variable (see Fig. 10)	
Applied torque	M_t [Nm]	10
Running speed	n [min^{-1}]	1000
Density (POM)	ρ [kg/m^3]	1410
Elastic modulus (POM)	E [MPa]	2600
Poisson ratio (POM)	ν [/]	0.3
COF (POM-POM)	μ [/]	0.21
Specific heat (POM)	c_p [J/(kgK)]	1470
Diffusivity (POM)	α [m^2/s]	$0.11 \cdot 10^{-6}$

Please cite this article as: B. Černe, J. Duhovnik and J. Tavčar, Semi-analytical flash temperature model for thermoplastic polymer spur gears with consideration of linear thermo-mechanical material characteristics, Journal of Computational Design and Engineering, https://doi.org/10.1016/j.jcde.2019.03.001

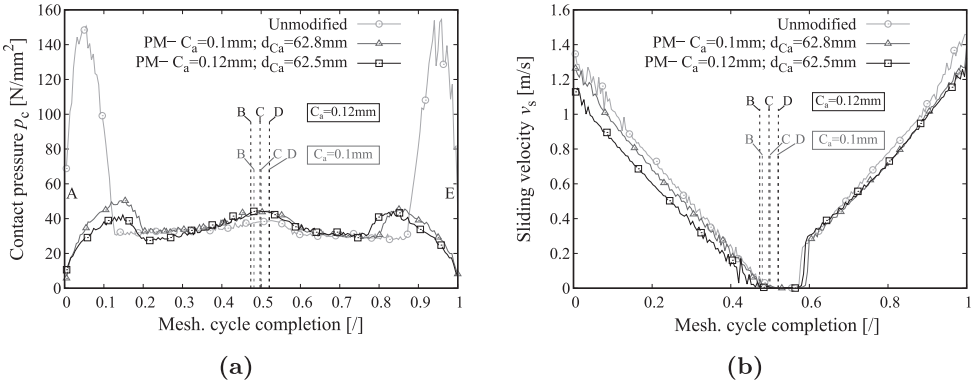

Fig. 10. Comparison between unmodified gear geometry and two degrees of profile modification for the gear pair defined in Table 4: evaluated contact pressures with FEA (a) and sliding velocities (b).

triple-tooth-pair contact. Additionally, the evaluated sliding speeds presented in Fig. 10b also show a noticeable drop in values for the modified geometries, especially in the first half of the meshing cycle. We also noticed that the meshing cycle times decrease if a profile modification is used (up to 16% between unmodified tooth and $C_a = 0.12$ mm modification).

On comparing the computed flash temperature patterns presented in Fig. 11 with the ones presented in Mao (2007) (see Appendix B), we note that the results for the modified profile geometries agreed with the cited work to a greater extent. It is necessary to consider that the pressures evaluated using the unmodified gear geometry would quickly result in permanent deformation as the yield strength of the material (typically for POM $R_m \approx 65$ MPa) is substantially exceeded. Hence, a running-in phase would likely occur wherein these overstresses would gradually phase out. It is thus of paramount importance to consider a suitable tip modification when using the presented model, as the material compliance typical for plastics otherwise results in deviations from the theoretical kinematics of the gear pair and consequently increased stresses that can be considered to be unrealistic for a steady-running-conditions case. Given our findings, we also highly recommend the implementation of suitable profile modifications when designing real-life polymer-gear applications. The results in Mao (2007) do not show any sudden spikes in flash temperature even though an unaltered gear geometry is considered because a theoretical load distribution is considered where the tip-jamming effect described previously is not recognised. Using FEA for the mechanical analysis we hence obtain a more faithful representation of the real life contact pressures and other related parameters that influence the generated heat losses.

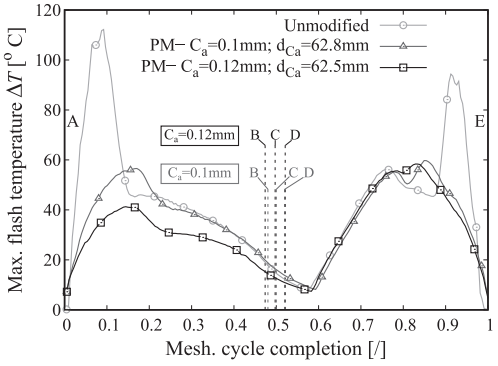

Fig. 11. Evaluated peak flash temperatures. The results obtained are comparable to those presented in Mao (2007).

5. Conclusion

The work provides an improved flash temperature model based on a combination of analytical and numerical tools, that accurately describes the contact conditions present during gear meshing, and hence enables a more realistic evaluation of the heat losses due to friction and of the consequent temperature rise.

Considering the results presented in this study, we can conclude that the overall evaluation of the flash temperature is dependent on several factors. Using the available mechanical, thermal, and frictional property data, we can calculate the contact pressure and contact interface size as time-dependent variables using FEA and evaluate the sliding speeds using a custom routine. These results enable us to calculate the heat flux entering the bodies at the contact area owing to frictional energy dissipation. The heat flux is distributed in the contacting bodies by a specific partitioning factor, which is defined using the presumption of equal temperature at the contacting interface for both bodies. The thermal load and thermal properties of the considered materials dictate the temperature rise during the gear meshing cycle. Based on the heat equation, a transient thermal analysis can be performed using numerical and analytical computation tools to evaluate the flash temperature progression during a gear meshing cycle. The developed model was validated using the results available in the literature, with which the obtained results coincide well if the teeth profiles are suitably designed. It was shown that it is of great importance to provide an appropriate profile modification of the tooth tip as the low stiffness of the considered polymers can result in substantial root deformations of the gear teeth and a deterioration of the system kinematics (even jamming in some cases). This was found to produce large contact stresses that can quickly exceed the yield strength of the material, which would result in permanent plastic deformations in real-life applications.

The advantage of the developed model is that it can be used on any type and size of spur-gear pair, including non-involute spur-gear types. The model however presumably shows realistic results only for moderate loading conditions wherein a quasi-steady nominal temperature state can be reached. If the power inputs are too high we can expect a so-called negative feedback loop where a substantial strain accumulation would occur owing to the viscoelastic properties of the polymers. This will inevitably result in further deviation from the ideal gearing kinematics, higher contact loads, and consequently increased local contact temperatures (which in turn would negatively affect the mechanical properties of these materials). It is, however, not typical to use such high loads in real-life applications, as the objective is generally to achieve a reasonable gear-train service life. For such applications, the developed computation tool can yield valuable information for

Please cite this article as: B. Černe, J. Duhovnik and J. Tavčar, Semi-analytical flash temperature model for thermoplastic polymer spur gears with consideration of linear thermo-mechanical material characteristics, Journal of Computational Design and Engineering, https://doi.org/10.1016/j.jcde.2019.03.001

the prediction of the long-term nominal and, hence, the overall temperature rise, which is a decisive criterion for the design of a high-performance polymer gear system.

Acknowledgment

The presented research was partly funded by the Slovenian Research Agency (ARRS) and partly covered with funds derived from the MAPgears project.

Appendix A. General description of the flash temperature increase due to a moving heat source

An analytical description of the flash temperature increase in a given body owing to a heat source passing at given speed is derived based on the following heat equation (Skinner, 2014):

$$\frac{\partial T(\mathbf{x},t)}{\partial t} = \alpha \nabla^2 T(\mathbf{x},t), \tag{A.1}$$

where T denotes temperature, t denotes time, $\mathbf{x}$ is the coordinate vector, and α is the thermal diffusivity. We first consider the 1D form $\partial T(x,t)/\partial t = \alpha \cdot \partial^2 T(x,t)/\partial x^2$, wherein the initial value problem on $\mathbb{R}^1 \times (-\infty,\infty)$ is defined by an initial temperature state $T(x,0) = h(x)$. We can obtain a solution for this problem using the Green's function principle. The key tool here is the Fourier transform, which can be applied to the differential terms in the equation as follows. In terms of the spatial coordinate, we obtain

$$\mathcal{F}\left\{\alpha \frac{\partial^2 T(x,t)}{\partial x^2}\right\} = \alpha \int_{-\infty}^{\infty} \frac{d^2 T(x,t)}{dx^2} \exp(-i2\pi f x)dx = -(2\pi f)^2 \alpha \hat{T}(f,t), \tag{A.2}$$

where $\hat{T}(f,t)$ is the Fourier transform temperature function. With respect to the time component, the Fourier transform is simply given as

$$\mathcal{F}\left\{\frac{\partial T}{\partial t}\right\} = \frac{\partial \hat{T}}{\partial t}. \tag{A.3}$$

Thus, we obtain the following first order differential equation:

$$\frac{\partial \hat{T}(f,t)}{\partial t} = -(2\pi f)^2 \alpha\, \hat{T}(f,t). \tag{A.4}$$

On considering that $\hat{T}(f,0) = \mathcal{F}\{h(x)\} = \hat{h}(f)$, the solution of the previous differential equation is

$$\hat{T}(f,t) = \hat{h}(f) \exp\left(-4\pi^2 f^2 \alpha t\right). \tag{A.5}$$

The solution of the 1D heat equation can be obtained by using the inverse Fourier transform as follows:

$$\mathcal{F}^{-1}\left\{\exp\left(-4\pi^2 f^2 \alpha t\right)\right\} = \frac{1}{\sqrt{4\pi\alpha t}} \exp\left(-\frac{x^2}{4\alpha t}\right) := S_n(x,t), \tag{A.6}$$

$$T(x,t) = \mathcal{F}^{-1}\left\{\hat{h}(f)\exp\left(-4\pi^2 f^2 \alpha t\right)\right\} = h(x) * \left[\frac{1}{\sqrt{4\pi\alpha t}} \exp\left(-\frac{x^2}{4\alpha t}\right)\right], \tag{A.7}$$

$$T(x,t) = \frac{1}{\sqrt{4\pi\alpha t}} \int_{-\infty}^{\infty} h(x') \exp\left[-\frac{(x-x')^2}{4\alpha t}\right] dx'. \tag{A.8}$$

As noted in Skinner (2014), the solution can be applied to the 3D heat Eq. (A.1) on $\mathbb{R}^3 \times (-\infty,\infty)$ as

$$T(\mathbf{x},t) = \frac{1}{(4\pi\alpha t)^{3/2}} \int_{\mathbb{R}^3} h(\mathbf{x}') \exp\left(-\frac{|\mathbf{x}-\mathbf{x}'|^2}{4\alpha t}\right) d^3x', \tag{A.9}$$

where $\mathbf{x} = (x,y,z)$. In a limiting case, where as an initial condition a finite amount of heat E_h is instantaneously released at point $\mathbf{x} = 0$ (with initial temperature being 0), the solution can be simply given as

$$\Delta T(\mathbf{x},t) = \frac{E_h}{\rho c_p (4\pi\alpha t)^{3/2}} \int_{\mathbb{R}^3} \delta(\mathbf{x}') \exp\left(-\frac{|\mathbf{x}-\mathbf{x}'|^2}{4\alpha t}\right) d^3x',$$

where ρ and c_p are the density and specific heat respectively, and hence

$$\Delta T(\mathbf{x},t) = \frac{E_h}{\rho c_p (4\pi\alpha t)^{3/2}} \exp\left(-\frac{|\mathbf{x}-\mathbf{x}'|^2}{4\alpha t}\right), \tag{A.10}$$

where $\delta(\mathbf{x}')$ represents the Dirac delta function. If the solid moves in the x-direction with a speed v, such that it's coordinates are $\{x - v(t-t'), y, z\}$, and a heat magnitude $Q \cdot dt'$ is released at t', the temperature at $T(\mathbf{x},t)$ is

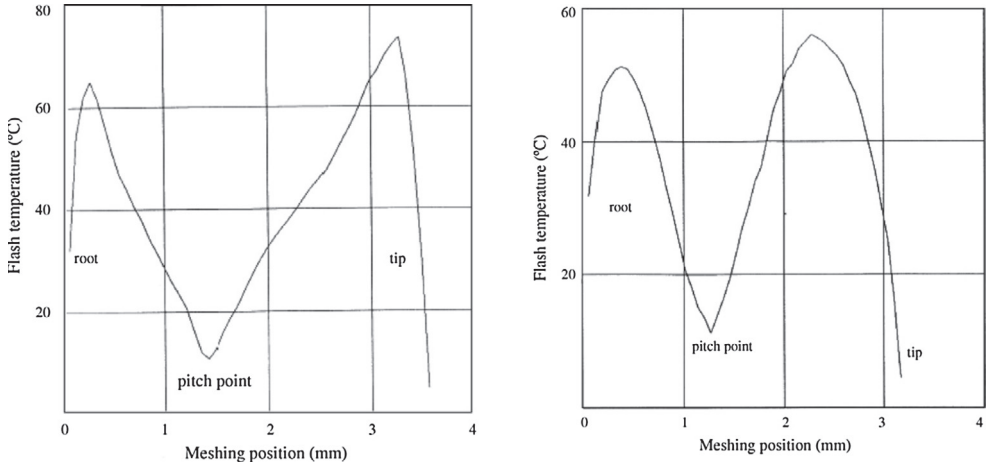

(a) Jump transition from double- to single-tooth contact

(b) Linear transition from double- to single-tooth contact

Fig. 12. Maximal flash temperature profiles evaluated in Mao (2007) for two types of theoretical contact pressure distributions.

Please cite this article as: B. Černe, J. Duhovnik and J. Tavčar, Semi-analytical flash temperature model for thermoplastic polymer spur gears with consideration of linear thermo-mechanical material characteristics, Journal of Computational Design and Engineering, https://doi.org/10.1016/j.jcde.2019.03.001

$$\Delta T(\mathbf{x},t)=\frac{Qdt'}{\rho c_p[4\pi\alpha(t-t')]^{3/2}}\exp\left\{-\frac{[x-v(t-t')]^2+y^2+z^2}{4\alpha t}\right\}. \tag{A.11}$$

If, instead, the heat rate Q is released during time 0 to t, the above formulation can, according to Carslaw and Jaeger (1959), be written as

$$\Delta T(\mathbf{x},t)=\frac{Q}{8\rho c_p(\pi\alpha)^{3/2}}\int_0^t\frac{1}{(t-t')^{3/2}}\times\exp\left\{-\frac{[x-v(t-t')]^2+y^2+z^2}{4\alpha t}\right\}dt'. \tag{A.12}$$

Appendix B. Flash temperature results from Mao (2007) used for the validation procedure

In Fig. 12 we present the results from the work Mao (2007) used for our model validation procedure presented in Section 4.3. The results in Fig. 12a show the maximal flash temperature pattern if a jump from double- to single-tooth contact (which in terms leads to a jump in contact pressures) is considered. Fig. 12b, on the other hand, shows results if a gradual shift from double- to single-tooth contact and a more gradual linear change in contact pressures is considered. As we have seen from our FEA results (see Fig. 4a) the contact pressure patterns during polymer gear meshing are neither linear nor a jump function. We can, however, still observe rather comparable results between our model (if tip profile corrections are implemented to smooth out pressure spikes) and the one used in the cited work.

Appendix C. Supplementary material

Supplementary data associated with this article can be found, in the online version, at https://doi.org/10.1016/j.jcde.2019.03.001.

References

Anderson, E., Bai, Z., Bischof, C., Blackford, S., Demmel, J., Dongarra, J., ... Sorensen, D. (1999). *LAPACK users' guide* (3rd ed.). Philadelphia, PA: Society for Industrial and Applied Mathematics.

ANSYS. (2018). *Mechanical APDL, Contact Technology Guide*, Source: <https://www.sharcnet.ca/Software/Ansys/16.2.3/en-us/help/ans_ctec/ctectoc.html> (Accessed: 25.10.2018).

Bansal, D. G., & Streator, J. L. (2011). On estimations of maximum and average interfacial temperature rise in sliding elliptical contacts. *Wear, 278-279*, 18–27. https://doi.org/10.1016/j.wear.2011.12.006.

Beermann, S. (2015). VDI 2736 – New guideline, old challenges. In *International Conference on Gears 2015 VDI-Berichte* (vol. 2255, pp. 1231—1240).

Blok, H. (1963). The flash temperature concept. *Wear, 6*, 483–494. https://doi.org/10.1016/0043-1648(63)90283-7.

Bos, J., & Moes, H. (1995). Frictional heating of tribological contacts. *Journal of Tribology, 117*, 171–177. https://doi.org/10.1115/1.2830596.

Burden, R. L., & Faires, J. D. (2011). *Numerical analysis* (9th ed.). Boston: Brooks/Cole, Cengage Learning.

Carslaw, H. S., & Jaeger, J. C. (1959). *Conduction of heat in solids* (2nd ed.). Oxford, London: Clarendon Press.

Duhovnik, J., Zorko, D., & Sedej, L. (2016). The effect of the teeth profile shape on polymer gear pair properties. *Technical Gazette, 23*, 199–207.

Erhard, G. (2006). *Designing with plastics*. Munich: Carl Hanser Verlag.

Fernandes, C. M. C. G., Rocha, D. M. P., Martins, R. C., & Magalhaes, L. (2018). Finite element method model to predict bulk and flash temperatures on polymer gears. *Tribology International, 120*, 255–268. https://doi.org/10.1016/j.triboint.2017.12.027.

Greenwood, J. A., Minshall, H., & Tabor, D. (1961). Hysteresis losses in rolling and sliding friction. *Proceedings of the Royal Society of London A: Mathematical, Physical and Engineering Sciences, 259*(1299), 480–507. https://doi.org/10.1098/rspa.1961.0004.

Hachmann, H., & Strickle, E. (1966). Polyamide als zahnradwerkstoffe. *Konstruktion, 18*, 81–94.

Hooke, C. J., Mao, K., Walton, D., Breeds, A. R., & Kukureka, S. N. (1993). Measurement and prediction of the surface temperature in polymer gears and its relationship to gear wear. *Journal of Tribology, 115*, 119–124. https://doi.org/10.1115/1.2920964.

Kennedy, F. E. (1984). Thermal and thermomechanical effects in dry sliding. *Wear, 100*, 453–476. https://doi.org/10.1016/0043-1648(84)90026-7.

Kennedy, F. E. (2001). Frictional heating and contact temperatures. In B. Bhushan (Ed.), *Modern tribology handbook, two volume set*. Boca Raton: CRC Press. Ch. 6.

Kennedy, F. E., Lu, Y., & Baker, I. (2015). Contact temperatures and their influence on wear during pin-on-disk tribotesting. *Tribology International, 82*(B), 534–542. https://doi.org/10.1016/j.triboint.2013.10.022.

Kennedy, T., Plengsaard, C., & Harder, R. (2006). Transient heat partition factor for a sliding railcar wheel. *Wear, 261*(7), 932–936. https://doi.org/10.1016/j.wear.2006.01.016.

Ling, F. F., Lai, W. M., & Lucca, D. A. (2002). *Fundamentals of surface mechanics, with applications* (2nd ed.). New York: Springer-Verlag.

Li, W., Zhai, P., Tian, J., & Luo, B. (2018). Thermal analysis of helical gear transmission system considering machining and installation error. *International Journal of Mechanical Sciences, 149*, 1–17. https://doi.org/10.1016/j.ijmecsci.2018.09.036.

Maitra, G. M. (2001). *Handbook on gear design*. New Delhi: Tata McGraw-Hill.

Mao, K. (1993). The performance of dry running non-metallic gears'. Ph.D. thesis. The University of Birmingham.

Mao, K. (2007). A numerical method for polymer composite gear flash temperature prediction. *Wear, 262*(11), 1321–1329. https://doi.org/10.1016/j.wear.2007.01.008.

Mao, K. (2007). A new approach for polymer composite gear design. *Wear, 262*(3), 432–441. https://doi.org/10.1016/j.wear.2006.06.005.

Myshkin, N., Petrokovets, M., & Kovalev, A. (2005). Tribology of polymers: Adhesion, friction, wear, and mass-transfer. *Tribology International, 38*, 910–921. https://doi.org/10.1016/j.triboint.2005.07.016.

Persson, B. N. J. (2000). *Sliding friction, physical principles and applications* (2nd ed.). Berlin, Heidelberg, New York: Springer.

Pogačnik, A. (2013). Effect of physical parameters on tribological properties of polymers for gears, Doctoral thesis. Ph.D. thesis. University of Ljubljana.

Pogačnik, A. & Tavčar, J. (2016). Accelerated testing and temperature calculation of plastic gears, gear solutions, December 15, 2016, Source: <http://gearsolutions.com/media/uploads/uploads/assets/Digital_Editions/201612/1216-KISSsoft.pdf> (Accessed: 28.8.2018).

Pogačnik, A., & Tavčar, J. (2015). An accelerated multilevel test and design procedure for polymer gears. *Materials and Design, 65*, 961–973. https://doi.org/10.1016/j.matdes.2014.10.016.

Savitzky, A., & Golay, M. J. E. (1964). Smoothing and differentiation of data by simplified least squares procedures. *Analytical Chemistry, 38*(8), 1627–1639. https://doi.org/10.1021/ac60214a047.

Scaraggi, M., & Persson, B. N. J. (2014). Rolling friction: Comparison of analytical theory with exact numerical results. *Tribology Letters, 55*(1), 15–21. https://doi.org/10.1007/s11249-014-0327-y.

Shojaei, A.,K., Volgers, P., & Morris, M. (2017). Advanced modeling and experimental techniques for fatigue life prediction of plastic gears. In *Proceedings from the VDI international conference on high performance plastic gears*.

Skinner, D. (2014). Mathematical methods, Green's functions for PDE's, Lecture notes, Department of Applied Mathematics and Theoretical Physics, University of Cambridge, Source: <http://www.damtp.cam.ac.uk/user/dbs26/1Bmethods.html> (Accessed: 26.10.2018).

Steiner, J., Termonia, Y., & Deltour, J. (1972). Smoothing and differentiation of data by simplified least square procedure. *Analytical Chemistry, 44*(11), 1906–1909. https://doi.org/10.1021/ac60319a045.

Sun, J., Sawley, K., Stone, D., Teter, D. (1998). Progress in the reduction of wheel spalling. In *Proceedings of the 12th international wheelset congress, Qingdao, China*.

Takanashi, S. & Shoi, A. (1980). On the temperature risk in the teeth of plastic gears. In *International power transmission and gearing conference, San Francisco*.

Tian, X., & Kennedy, F. E. (1993). Contact surface temperature models for finite bodies in dry and boundary lubricated sliding. *Journal of Tribology, 115*, 411–418. https://doi.org/10.1115/1.2921652.

Tian, X., & Kennedy, F. E. (1994). Maximum and average flash temperatures in sliding contacts. *Journal of Tribology, 116*, 167–174. https://doi.org/10.1115/1.2927035.

VDI 2736-Blatt 2:2014-06, Thermoplastic gear wheels – Cylindrical gears – Calculation of the load-carrying capacity.

Wannop, G. L., & Archard, J. R. (1973). Elastic hysteresis and a catastrophic wear mechanism for polymers. *Proceedings of the Institution of Mechanical Engineers, 187*(1), 615–623. https://doi.org/10.1243/PIME_PROC_1973_187_147_02.

Williams, J. A., & Dweyer-Joyce, R. S. (2000). Contact between solid surfaces. In B. Bhushan (Ed.), *Modern tribology handbook two volume set*. Boca Raton: CRC Press. Ch. 6.

Zeller, C., Surendran, B., & Zaeh, M. F. (2018). Parameterized extended finite element method for high thermal gradients. *Journal of Computational Design and Engineering, 5*(3), 329–336. https://doi.org/10.1016/j.jcde.2017.12.001.

Zorko, D., Kulovec, S., Tavčar, J., & Duhovnik, J. (2017). Different teeth profile shapes of polymer gears and comparison of their performance. *Journal of Advanced Mechanical Design, Systems and Manufacturing, 6*(11), 1–10. https://doi.org/10.1299/jamdsm.2017jamdsm0083.

Please cite this article as: B. Černe, J. Duhovnik and J. Tavčar, Semi-analytical flash temperature model for thermoplastic polymer spur gears with consideration of linear thermo-mechanical material characteristics, Journal of Computational Design and Engineering, https://doi.org/10.1016/j.jcde.2019.03.001